Journal of Applied Fluid Mechanics, Vol. 18, No. 1, pp. 2599-2609, 2025.
Available online at www.jafmonline.net, ISSN 1735-3572, EISSN 1735-3645.
https://doi.org/10.47176/jafm.18.10.3427

Experimental Investigation of the Flow Resistance Characteristics of Air Vertically Flowing through a Horizontal Tube Bundle with Falling Film Water

C. Li, X. Zhang, Y. Guo, S. Shen†, and Q. Qiu

State-Local Joint Engineering Research Center of Thermal Energy Comprehensive Utilization Technologies, Dalian University of Technology, Dalian, Liaoning Province, 116024, China

†*Corresponding Author Email: zzbshen@dlut.edu.cn*

ABSTRACT

The pressure drops and the friction factor of the air flowing up and down through a horizontal tube bundle with falling film water are investigated in this work, and the effects of air velocity, water spray density and air flow direction are studied. The experiment is conducted on a 13-row horizontal tube bundle with a tube diameter of 38 mm and a total of 33 tubes. The experimental data covers an air velocity range of 2.5~6.4 m/s, a water spray density range of 0.056~0.111 kg/(m·s), an air temperature of 20 °C, an air relative humidity of 60% and a spray water temperature of 30 °C. The pressure drop has a positive relationship with the spray density and air velocity, and the counter flow has a slightly larger pressure loss compared with the cocurrent flow. The proportions of the pressure drop caused by the friction between the air and spray water to the total pressure are observed to increase with the spray density and decrease with the air velocity for both counter and cocurrent flow. These proportions for the two flow patterns are approximately 10~30% for counter flow and 10~25% for cocurrent flow, respectively. Based on experimental data, prediction correlations of the friction factors through horizontal falling film tube bundles are proposed, and the prediction deviation for almost all experimental data is within ±5%.

Article History

Received February 2, 2025
Revised April 19, 2025
Accepted May 4, 2025
Available online August 5, 2025

Keywords:

Pressure drop
Friction factor
Prediction correlation
Evaporative condenser
Counterflow
Cocurrent flow

1. INTRODUCTION

Condensers are widely used in various industrial fields and can be divided into air-cooling, water-cooling and evaporative-cooling types. The evaporative condenser is gaining traction in some cases; it uses less circulating cooling water than the water-cooling condenser does and has a better cooling capacity than the air-cooling condenser does, especially in summer, when the air temperature is high (Skundric et al., 2023). In a tube-type evaporative condenser, heat is released by condensation inside tubes and transferred to the low-temperature water film covering the tubes, which is in the form of a falling film flow pattern.

Most studies on evaporative condensers focus on their heat and mass transfer performance. Mizushina et al. (1967) conducted experiments on counterflow evaporative condensers with 12.7-, 19.05- and 40-mm-dia coils to determine the influence of tube size on the heat and mass transfer coefficients. Zalewski and Gryglaszewski (1997) presented a mathematical model of an evaporative condenser with countercurrent air flow, and the calculated results of heat and mass transfer were in satisfactory agreement with the experimental data of a water evaporative condenser. Heyns and Kröger (2010) reported correlations of the heat and mass transfer coefficients of a water film based on the experiments conducted on a 15-row-tube evaporative condenser. They also noted the influential factors of heat and mass transfer and pressure drop. Anderson (2014) experimentally studied the heat transfer and air flow characteristics of a counterflow test section in a hybrid dry/wet dephlegmator and reported the correlations of the heat transfer coefficient and air-side pressure drop coefficient. Zhang et al. (2023) conducted an experiment on an evaporative condenser with cocurrent air flow and obtained correlations of the heat and mass transfer coefficients.

The air-side pressure drop is an important parameter in the design and analysis of evaporative condensers. It determines the power consumption of the device. However, research on the flow resistance of horizontal tube falling film evaporative condensers is insufficient (Plessis & Owen, 2020). Finlay and Harris (1984) measured

NOMENCLATURE

A	flow area	X_{tt}	Martinelli parameter
D	tube diameter	Γ	spray density per side
f	friction factor	μ	dynamic viscosity
G	mass velocity	ρ	density
m	mass flowrate	**Subscript**	
ΔP	pressure difference	g	gas
Re	Reynolds number	l	liquid
s/D	tube pitch between the center of two adjacent tubes	tp	two-phase flow
T	temperature	tb	tube bundle
v	gas velocity	ctr	counter flow
v^*_g	equivalent gas velocity	cot	cocurrent flow
V	volume flowrate	st	steam
x	quality	sat	saturated

the pressure loss of the air flowing across horizontal coils in an evaporative condenser and reported the pressure drop correlations of plain and finned tube bundles, considering the air mass velocity, spray density and tube size. Heyns and Kröger (2010) also obtained the air-side pressure drop correlation in their experiments, which is a function of the air and sprayed water mass flow rates. Plessis and Owen (2020) experimentally investigated the pressure drop of counterflow air flowing across a horizontal tube bundle under both dry and wet conditions.

Catrawedarma & Deendarlianto (2020) conducted deep studies on multiphase flow in the vertical direction. The experimental, theoretical, and numerical studies on the flow characteristics of multiphase flow in airlift pumps were comprehensively summarized. Their study reveals that the pressure drop in two-phase flow conditions is affected by a variety of forces, including water pressure, weight, and friction force, and new directions for future research were also proposed. Furthermore, a novel mechanism model for determining the velocity of discharged surface water was proposed through the force balance method and dimensional analysis (Catrawedarma & Deendarlianto, 2022).

The pressure drop correlations used in these studies are listed in Table 1. However, these correlations are dimensional, or the two sides of the correlations are not equal in dimension, which makes them less applicable to cases beyond their conditions.

The dimensionless form of the air-side pressure drop prediction correlation can be found in some similar studies. Some researchers have studied the pressure loss characteristics of gas horizontally flowing through horizontal tube bundles with water spraying. Liu et al. (2014) designed experiments to research the 50~70 °C saturated steam pressure drop in crossflow in a falling film bundle, and the spray water density ranged from 0.02 kg/(m·s) to 0.08 kg/(m·s). The pressure drop was divided into two parts: the pressure drop caused by the tube bundle and the spray liquid column. The Reynolds numbers of spray water and steam were suggested to be parameters of the pressure drop prediction correlation, which could predict experimental data within a deviation of ±10%. A similar correlation form can be found in the research reported by She et al. (2021), in which the pressure drop was also divided into two parts. A correlation involving the ratio of the liquid and gas Reynolds numbers, X_{tt}, the Froude number, the gas velocity and other physical and structural parameters was used to calculate the pressure drop caused by the spray liquid, and the single-phase pressure drop was also calculated in the form of Blasius-type equation (Xu et al., 1998). The correlations of these two studies are listed in Table 2.

Table 1 Correlations of air-side pressure drop between horizontal tube bundle in evaporative condenser

Scholars	correlation	fluids	condition
Finlay and Harris (1984)	$\frac{\Delta p}{Z}=4.9G_{air}^{1.85}\left(\frac{\Gamma}{D_o}\right)^{0.285}$ *Z is the vertical length of the tube bundle.	water, air	D_o=38.1 mm, 2≤G_{air}≤6 kg/(m²·s), 1.3≤Γ/D_o≤3.5 kg/(m²·s), plain tube bundle
Heyns and Kröger (2010)	$\Delta p=10.2G_{air}^{1.8}G_{water}^{0.22}$	water, air	D_o=38.1 mm, 0.7≤G_{air}≤3.6 kg/(m²·s), 1.8≤G_{water}≤4.7 kg/(m²·s), s/D_o=2, triangular staggered array
Plessis and Owen (2020)	$f=(C_1G_{air}^{C_2}G_{water}^{C_3}+C_4G_{air}^{C_5}G_{water}^{C_6})\times C_7\left(\frac{D_o}{N}\right)^{C_8}+C_9e^{\frac{G_{water}}{G_{air}}}$ *N is the number of tubes; C_1~C_9 are constants.	water, air	19≤D_o≤25 mm, 1≤G_{air}≤3 kg/(m²·s), 2≤G_{water}≤4 kg/(m²·s), s/D_o=2, triangular staggered array

Table 2 Correlations of air-side pressure drop between horizontal tube bundle in similar research field

Scholars	correlation	fluids	condition
Liu et al. (2014)	$f=1.4Re_{st}^{-0.15}+6.8Re_{st}^{-0.77}Re_{\Gamma}^{0.69}$	water,steam	D_o=25.4 mm, 0.02≤Γ≤0.08 kg/(m·s), 50≤T_{sat}≤70 °C, triangular staggered array
She et al. (2021)	$f=41.37Re_{air\_dry}^{-0.45551}+C_dP$ $P=\left(-2.929+2.034X_{tt}^{0.386}\left(\frac{Re_l}{Re_{air\_wet}}\right)^{-0.336}(Fr_{air})^{0.00522}\right)^2$ * C_d is the pressure drop coefficient of circular cylinder	water,air	D_o=25.4 mm, Re_{gd}=1570~7850, Re_{gw}=1570~7850, Re_l=30~200, s/D_o=1.3, triangular staggered array

The prediction of the air-side pressure variation between the tube bundle is a significant research point, as it is closely tied to the energy consumption of the evaporative condenser and the proper selection of the pump. Moreover, current air-side pressure drop correlations are dimensional, which increases the difficulty in terms of their adaptability to other cases beyond the test conditions. To address these challenges, this study aims to investigate the air-side pressure drop characteristics between falling film tube bundles and reveal the influence mechanisms of spray density, airflow velocity, and flow direction on the pressure drop, as well as the mechanism of the coupling effects of these factors. In addition, dimensionless friction factor correlations for both single-phase and spray conditions are proposed to address the lack of research on air-side pressure drop prediction, overcoming the limitations regarding practical application in engineering. This study can also provide experimental data and research ideas for studying this type of problem.

2. EXPERIMENTAL SETUP

2.1 Experiment System

The experiment system of air flowing vertically over the horizontal tube bundle with spray water falling is shown in Fig. 1. The experimental system mainly includes a tube bundle system, a spray water circulation system and an air supply system. When it works, the spray water falls on the tube bundle, then falls to the tank and is recycled to the spray tube. Air is driven by a fan and passes through the tube bundle with a falling film of spray water.

The tubes are fixed by tube sheets on both sides, which constitute the main pressure loss section, and the front and back of this section are transparent polycarbonate sheets used to observe the flow of spray water. Sealing rings and glass cement are used at the joints between tubes and tube sheets and between tube sheets and polycarbonate sheets to prevent air from flowing out. The outside diameter of the tubes is 38 mm, and the tube sheet is designed to correspond to a staggered arrangement with a relative tube pitch of 1.6, as shown in Fig. 2. There are a total of 33 tubes in 13 rows, and odd-numbered tube rows are set to ensure that the structure of the tube bundle is the same when the air flows through, regardless of whether the air flows upward or downward.

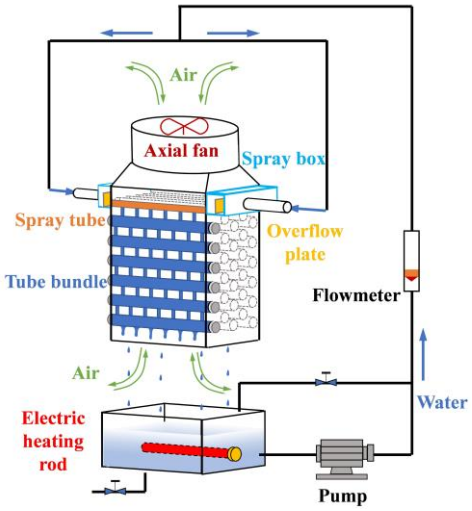

Fig. 1 Schematic of the experimental apparatus

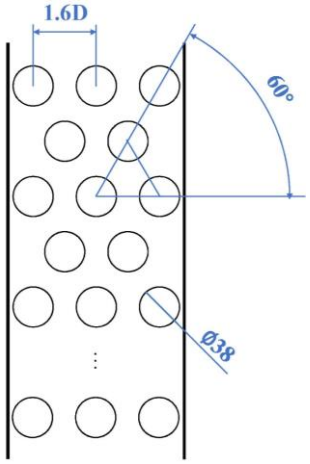

Fig. 2 Schematic of the tube arrangement

The spray water circulation system allows the spray water to fall and form a liquid film on the horizontal tube bundle, which consists of a tank, a water circulating pump and a spray device. An electric heating rod is used to maintain the temperature of the spay water in the tank at 30 °C. Considering the needs of the experiments, the pump is selected as a centrifugal pump, 25WBS2-8-0.25, with a rated flow rate of 2 t/h, a rated head of 8 m and a rated power of 250 W. In addition, the spray device includes

Table 3 Accuracies of measurement apparatus

variables	apparatus	type	range	accuracy
pressure difference	differential pressure transmitter	HALO-FY-WG	0~500 Pa	±1 Pa
volume flowrate of spray water	float flowmeter	LZS-15C	250~2500 L/h	±50 L/h
velocity of air	anemometer	AS836	0.3~45 m/s	±(1.5%rdg+0.1) m/s
temperature of spray water	thermocouple	T-type	−200~350 ℃	±0.05 ℃

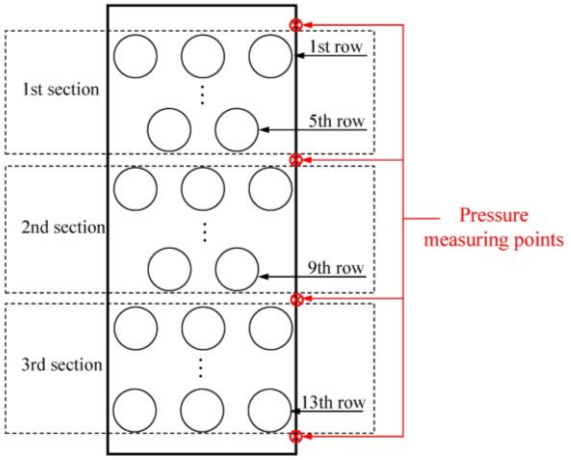

Fig. 3 Positions of the pressure difference measuring points

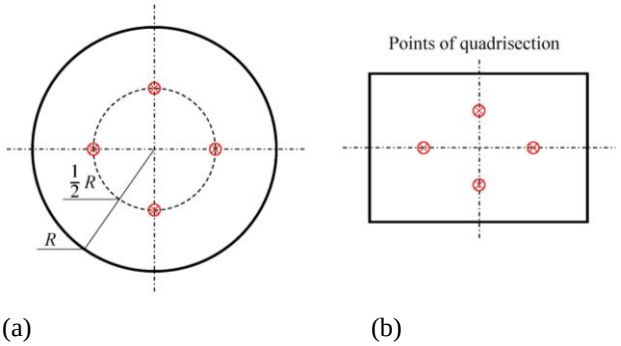

Fig. 4 Positions of the air inlet velocity measuring points in (a) air upper inlet and (b) air lower inlet

spray boxes and spray tubes. The spray box is designed with a structure similar to setting baffles perpendicular to the water flow direction in the tube header. This structure allows water to overflow into the spray tubes so that the flow state of the water is more stable when it enters the spray tubes. In addition, two identical spray boxes are arranged on both sides of the spray tube, and the water is pumped into both spray boxes at the same time to minimize the uneven spray density caused by supplying water on only one side as much as possible.

The air supply system provides stable air flow by an axial fan, which drives the air to flow up and down through the entire experimental facility. The axial fan is SF3-2 with a maximum air volume flow rate of 6000 m^3/h, a total pressure of 230 Pa and a rated power of 370 W. The power of the axial fan and the air flow direction are controlled by an inverter, YK-9000-7.5.

2.2 Measurement Apparatus

A wind pressure transmitter is used to measure the pressure difference of air passing through the tube bundle. There are 4 measuring points set on the polycarbonate sheets, which roughly divide the tube bundle into three sections at equal intervals. Thus, the pressure difference of each section and the total pressure difference can be obtained. The wind pressure transmitter, HALO-FY-WG, ranges from 0~500 Pa. The positions of the pressure difference measuring points are shown in Fig. 3.

The spray density is calculated by the volume flow rate of the spray water. The volume flow rate is measured by a float flowmeter, LZS-15C, which is set between the pump and the spray device and ranges from 250-2500 L/h.

The inlet velocity of the air is measured by an anemometer, AS836. There are 4 measuring points set at the air inlet, and the average of these air inlet velocities is considered the inlet velocity of the air. The positions of the measuring points of the air cocurrent flow and counter flow are shown in Fig. 4.

A T-type thermocouple is selected and placed in the water tank without contacting the wall of the tank to monitor the temperature of the spray water, which is precalibrated, and its accuracy reaches 0.05 °C.

The accuracies of the measurement apparatus are summarized in Table 3.

2.3 Scope of the Test

In the experiments, the air temperature was approximately 20 °C, the relative humidity of the air was approximately 60%, and the temperature of the spray water was maintained at 30 °C. The effective length of the tubes is 288 mm. The volume flow rate of spray water is 600~1200 L/h, corresponding to a spray density of 0.056~0.111 kg/(m·s). The inlet velocity of the air is 1.0~3.1 m/s, and the circulation area of the test section is 0.0555 m^2.

2.4 Data Reduction and Uncertainty Analysis

The spray density on one side of each tube can be obtained by Eq. (1).

$$\Gamma = \frac{\rho_l V_l}{2nL} \tag{1}$$

where ρ_l is the density of water, kg/m^3; V_l is the volume flow rate of water, m^3/s; n is the number of first row tubes; and L is the effective length of the tubes, m. In this study, n is 5, and L is 0.288 m.

The measured inlet velocity of air, $v_{g,\,inlet}$, should be corrected to reflect the real velocity because of the change

Table 4 Correspondence of the air inlet velocity $v_{g,\,inlet}$, inlet and equivalent velocity v^*_g, [m/s]

v^*_g	2.5	3.3	3.9	4.5	5.1	5.8	6.4
$v_{g,\,inlet,\,ctr}$	1.2	1.6	1.9	2.2	2.5	2.8	3.1
$v_{g,\,inlet,\,cot}$	1.0	1.3	1.5	1.7	2.0	2.2	2.4

in the flow area. According to the law of conservation of mass, the equivalent air velocity v^*_g can be obtained by multiplying $v_{g,\,inlet}$ with the ratio of the air inlet area A_{inlet} and the circulation area in the tube bundle $A_{tb,}$ as shown in Eq. (2), whereas the density of air can be considered constant.

$$\rho v_g^* = \rho v_{g,inlet} \cdot \left(A_{inlet} / A_{tb} \right) \tag{2}$$

The air inlet velocity of the upper inlet is set in reference to that of the lower inlet to ensure the same flow rate of the air flowing across the test section under both counterflow and cocurrent flow conditions. The correspondence of the air inlet velocity $v_{g,\,inlet}$ and equivalent velocity v^*_g is shown in Table 4.

The Reynolds numbers of falling film water (Re_Γ) and air (Re_g) are defined as follows:

$$Re_\Gamma = \frac{4\Gamma}{\mu_l} \tag{3}$$

$$Re_g = \frac{\rho v_g D}{\mu_g} \tag{4}$$

where μ_l is the dynamic viscosity of falling film water, Pa·s; v_g is the air velocity, m/s; D is the diameter of the tube, m; and μ_g is the dynamic viscosity of air, Pa·s.

The range of the differential pressure transmitter is 0~500 Pa with an accuracy of 1 Pa, and the minimum pressure difference in the experiments is 18 Pa. Thus, the uncertainty of the differential pressure transmitter is as follows:

$$\frac{\delta(\Delta p)}{\Delta p} = \frac{1}{18} \times 100\% = 5.56\%$$

The range of the float flowmeter is 250~2500 L/h with an accuracy of 50 L/h, and the minimum measured air velocity is 600 L/h. Thus, the uncertainty of the volume flow rate of spray water is as follows:

$$\frac{\delta(V)}{V} = \frac{50}{600} \times 100\% = 8.33\%$$

According to the propagations of uncertainty from the research of Kline (1985), the uncertainty of the spray density can be obtained by Eq. (5):

$$\frac{\delta(\Gamma)}{\Gamma} = \left[\left(\frac{\delta(V)}{V} \right)^2 + \left(\frac{\delta L}{L} \right)^2 \right]^{\frac{1}{2}} \tag{5}$$

where $\delta(L)/L$ is the uncertainty from the mechanical processing error of the tube, and this uncertainty is too small to affect the uncertainty of the spray density. Thus, the uncertainty of the spray density can be simplified as

$$\frac{\delta(\Gamma)}{\Gamma} = \left[\left(\frac{\delta(V)}{V} \right)^2 \right]^{\frac{1}{2}} = 10.42\%$$

The range of the anemometer is 0.3~45 m/s, with an error of ±(1.5%rdg+0.1) m/s, and the minimum measured air inlet velocity is 1.0 m/s. Thus, the uncertainty of the air velocity is:

$$\frac{\delta(v_g)}{v_g} = \frac{1 \times 1.5\% + 0.1}{1} \times 100\% = 11.5\%$$

The accuracy of the thermocouple is 0.05 °C, and the measured temperature is 30 °C. Thus, the uncertainty of the temperature is:

$$\frac{\delta(T)}{T} = \frac{0.05}{30} \times 100\% = 0.17\%$$

3. RESULTS AND ANALYSIS

Previous research has suggested that the pressure drop of a tube bundle with spray water is greater than that without spray water because there is an extra pressure drop caused by the liquid film on the tubes and the liquid between the tubes. Thus, the total pressure drop can be regarded as the sum of the pressure drop caused by the single-phase air flowing through the tube bundle and the pressure drop caused by spray water, which has also been analyzed by researchers such as Liu et al. (2014) and She et al. (2021). The pressure drop can be expressed as:

$$\Delta P = \Delta P_{tb} + \Delta P_\Gamma \tag{6}$$

where ΔP_{tb} is the single-phase pressure drop of air flowing across the tube bundle, and ΔP_Γ is the pressure drop caused by friction between the air and spray water.

3.1 Effects of the Air Velocity and Spray Density

The air velocity v^*_g and spray density both have positive effects on the pressure drop ΔP under the air counterflow and cocurrent flow conditions. The relation is described in Fig. 5, in which the subscript 'ctr' represents counter flow and 'cot' represents cocurrent flow. Under nonspray conditions, single-phase flow occurs in the tube with some obstacles, and the measured pressure drops are caused by the tube bundle; that is, ΔP is actually the pressure drop of the tube bundle, ΔP_{tb}, which is shown by black curves. For the spray condition, the ΔP under the counter flow condition depicted in Fig. 5(a) is slightly greater than that under the cocurrent flow condition illustrated in Fig. 5(b). To clarify the effects of the air velocity, spray density and flow direction on the pressure drop under spray conditions, the concept of the spray pressure drop ΔP_Γ is created, which is obtained by Eq. (6).

The absolute uncertainty of ΔP_Γ can be obtained by the Eq. (7):

$$U_{\Delta p_\Gamma} = \sqrt{U_{\Delta p}{}^2 + U_{\Delta p_{tb}}{}^2} \tag{7}$$

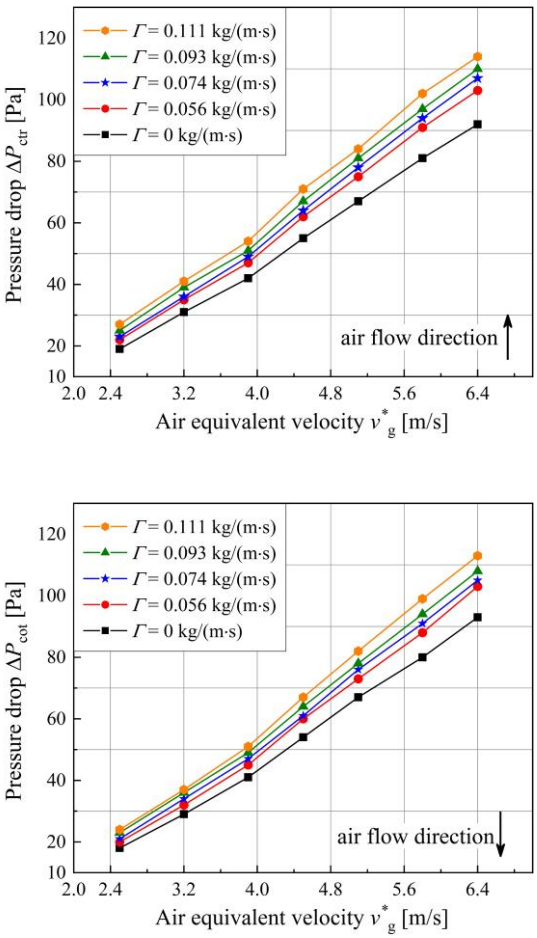

Fig. 5 Effect of the air velocity on the pressure drop at the different spray densities under (a) counterflow and (b) cocurrent flow conditions

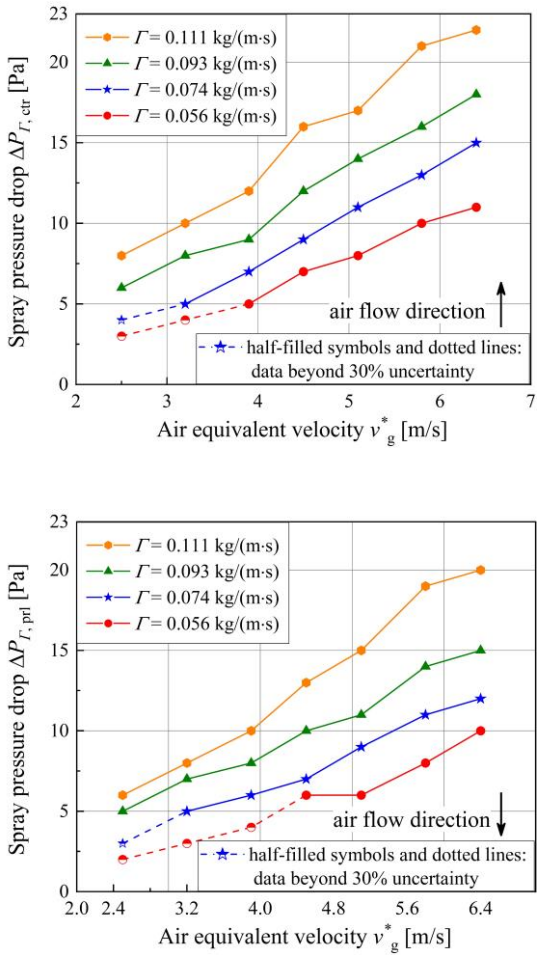

Fig. 6 Variation in the spray pressure drop under different air velocities and spray densities under (a) counterflow and (b) cocurrent flow conditions

and the absolute uncertainty is

$$U_{\Delta p_\Gamma} = \sqrt{1^2+1^2} = 1.41\,(\mathrm{Pa})$$

Under low-ΔP_Γ conditions, the value of ΔP_Γ may be so small that the uncertainties of some data exceed 30%, but these data points and curves are still reserved with marks in relevant figures to provide references.

As shown in Fig. 6, a higher air velocity results in a greater ΔP_Γ value, and the counter flow has a slightly larger ΔP_Γ value. One factor is that the higher-velocity airflow more violently disturbs the falling film of the spray water, which causes stronger friction at the interface of the air and spray water and results in a more direct impact between the air and spray water. Another factor is that the air flow disturbs the liquid columns or sheets into an unsteady flow state as the air velocity increases, which results in a higher local relative velocity and further causes more local pressure loss. Under counter flow conditions, air with a relatively high velocity hinders water from falling, which also results in strong shear and a surge in direct impact between the air and water because of the increase in water-film fluctuations and water splashing (Fiorentino & Starace, 2016).

The ΔP_Γ of the air flowing across the horizontal tube bundle also increases with the spray density of the water, regardless of whether the flow directions of the air and spray water are the same, as depicted in Fig. 6. This is because spray density influences ΔP_Γ such that the spray water falls on the horizontal tube and forms a liquid film, which hinders the area flowing through and further decreases the flow area of the air so that the local air velocity and friction loss both increase. Another way for the spray density influencing the pressure drop is that the falling film flow pattern of the spray water changes from column flow to sheet flow when the spray density changes from 0.056 to 0.111 kg/(m·s), which further decreases the area of air flow and increases the interaction between the air and spray water.

The proportions of ΔP_Γ in ΔP for both counterflow and cocurrent flow have a positive relationship with the spray density and a negative relationship with the air velocity, as described in Fig. 7. The proportion for counter flow is larger, approximately 10~30%, whereas that for cocurrent flow is approximately 10~25%. When the air velocity is fixed, ΔP_{tb} is constant, and a greater spray density results in a greater ΔP_Γ, which increases with

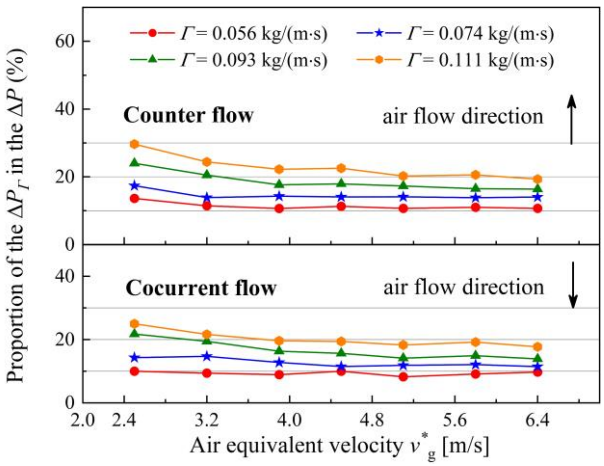

Fig. 7 Proportion of ΔP_Γ in ΔP for counter flow and cocurrent flow

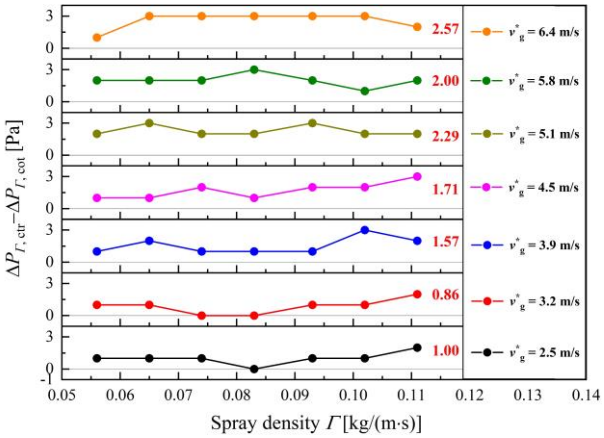

Fig. 8 Effect of the air flow direction on the spray pressure drop

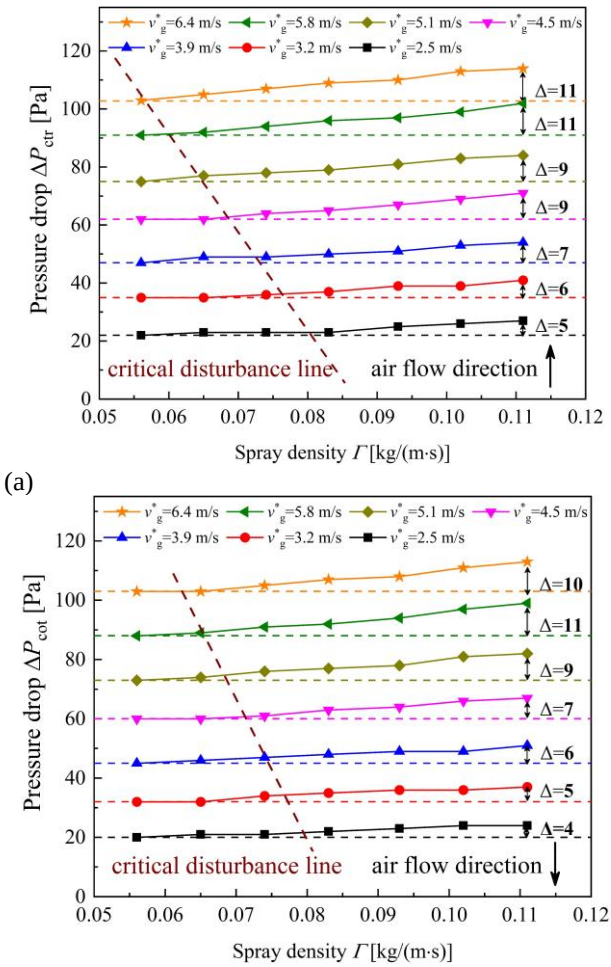

Fig. 9 Effect of the spray density on the pressure drop under different air velocities under (a) counterflow and (b) cocurrent flow conditions

increasing spray density. When the spray density is fixed, both ΔP_{tb} and ΔP_Γ increase with increasing air velocity, but the proportion decreases with increasing air velocity. This is because ΔP_{tb} has a quadratic relationship with the air velocity, but the slope of ΔP_Γ changes with air velocity is lower.

3.2 Reasons for the Slight Effect of the Air Flow Direction

The air flow direction has a slight influence on the pressure drop of the air, which is reflected partially in the above sections. The influence of the air flow direction mainly focuses on the spray pressure drop ΔP_Γ, and the differences between the ΔP_Γ values of counter flow and cocurrent flow are described in Fig. 8, in which the red numbers represent the average difference. The difference between the ΔP_Γ values of counter flow and cocurrent flow also increases with increasing air velocity, whereas the correlation between the difference in ΔP_Γ and spray density is not obvious. The close relative velocities between the spray water and air in the two flow directions are the key factors causing this result. Although the shear force at the air–water interface also exists under the cocurrent flow condition, which causes friction loss of the air, the relative velocity is slightly lower than that under the counterflow condition so that the friction strength of the cocurrent airflow is lower. The counter airflow results in more violent interactions between the airflow and the falling film water because it opposes the gravity of the liquid and causes the liquid flow pattern to change, resulting in liquid splashing or even blowing up the liquid, which further increases the ΔP_Γ to some extent. Thus, the pressure drop under counter flow conditions is slightly greater than that under cocurrent flow conditions. Furthermore, the increase in ΔP_Γ with increasing air velocity is more rapid than the linear increase is, resulting in a slight increase in the value of $\Delta P_{\Gamma,ctr}-\Delta P_{\Gamma,cot}$ with increasing air velocity.

3.3 Low- and High-Disturbance Regions

The increase in ΔP is not obvious at different velocities when the spray density is lower than a critical value, whereas ΔP increases with increasing air inlet velocity at higher spray densities. The critical disturbance lines, which consist of critical spray densities at different velocities, approximately divide the pressure drop region into two parts, as illustrated in both Fig. 9(a) and Fig. 9(b). The left region is the low-disturbance region, whereas the right region is the high-disturbance region. The disturbance of this mixed flow comes from two parts: the air reduces the stability of the spray water flow, and the degree of turbulence of the spray water increases with

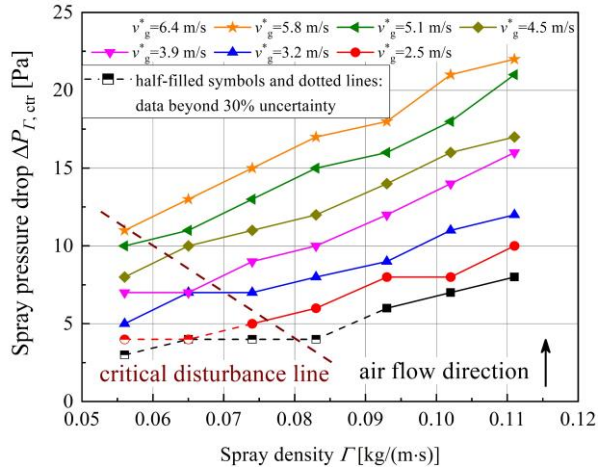

(a)

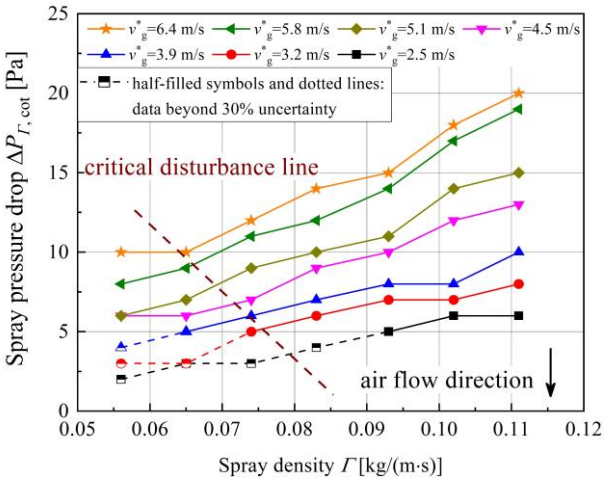

(b)

Fig. 10 Effect of the spray density on the spray pressure drop under different air velocities under (a) counterflow and (b) cocurrent flow conditions

increasing spray density. The air with a higher velocity and the spray water with a larger mass flux can both increase the integral disturbance to carry the flow into the high-disturbance region.

The distribution of the disturbance regions can be more clearly illustrated by the analysis of the influence of spray density on the spray pressure drop ΔP_Γ because the resistance from the falling film liquid actually influences ΔP_Γ, which is shown in Fig. 10. The ΔP_Γ increases relatively slowly in the low-disturbance region, which is on the left of the critical disturbance line. As the spray density increases, it enters the high-disturbance region, and ΔP_Γ increases relatively quickly. When the air velocity is relatively high, the disturbance from the air is sufficient to carry this mixed flow into the highly disturbance region and can result in a sharp increase in ΔP under a relatively low spray density. When the air velocity is lower, the disturbance from the air is not enough to achieve the transition so that it is waiting for an increase in the degree of turbulence of the water; that is, more spray density is needed to change the mixed flow into a highly disturbance region. In Fig. 10(b), the critical disturbance line moves slightly to the right because the same flow direction results in a lower relative velocity between the air and water, and the interaction between them consists of more shear but less direct impact, which causes less disturbance from the air for the cocurrent flow when the air velocity is the same. Thus, more spray density is needed under the cocurrent flow condition, which is not obvious when the air velocity is lower because the disturbance from the air occupies a small proportion.

3.4 Correlations of the Pressure Drop

The total pressure drop is the sum of the pressure drops caused by air flowing through each row of the tube bundle, and the mass velocity of the air flowing across each row of the tube bundle is the same. Thus, the total pressure drop can be obtained by Eq. (7):

$$\Delta P = N \cdot \frac{1}{2} f \rho v^2 = N \cdot \frac{1}{2} f \frac{G^2}{\rho} \tag{8}$$

where N is the number of tube rows (N=13); v is the velocity of the air, m/s; and G is the mass velocity of the air, kg/m^2·s. In addition, f can be calculated by Eq. (8):

$$f = \frac{1}{N} \frac{2\rho \Delta P}{G^2} \tag{9}$$

The total pressure drop consists of two parts, the single-phase pressure drop ΔP_{tb} and the pressure drop of air flowing across the spray water ΔP_Γ, as expressed in Eq. (6), which are analyzed below.

3.4.1 Single-phase Friction Factor

The single-phase friction factor is calculated via a Blasius-type equation, which is defined as:

$$f_{tb} = \frac{A}{Re_g^m} \tag{10}$$

where A and m are constants. Re_g is defined in Eq. (4), where the air velocity should be transformed into the equivalent air velocity v^*_g:

$$Re_g = \frac{\rho v_g^* D}{\mu_g}$$

The prediction correlations of the single-phase friction factors for counter flow and cocurrent flow under nonspray conditions are obtained based on the experimental data:

For counter flow:

$$f_{tb,ctr} = 6.287\, Re_g^{-0.3057} \tag{11}$$

For cocurrent flow:

$$f_{tb,prl} = 3.151 Re_g^{-0.2340} \tag{12}$$

The experimental single-phase friction factor is compared with the prediction of Eq. (10) and Eq. (11) and the research of Žukauskas (1972), which is shown in Fig. 11. The red and blue symbols ‘x’ represent the experimental friction factors of counter flow and cocurrent flow, respectively, and the black line is obtained by a

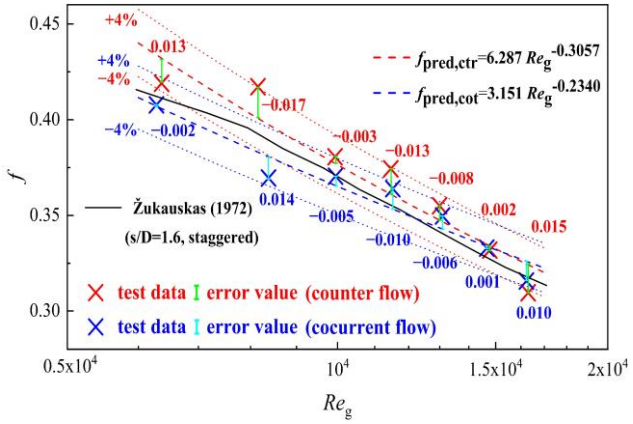

Fig. 11 Comparison of the experimental single-phase friction factor with the predictions of Eq. (11) and Eq. (12) and with Žukauskas' research

graphical method from Žukauskas's research. The red and blue dashed lines represent Eq. (10) and Eq. (11), respectively, while some dotted lines around these dashed lines represent the ± 4% deviation of the above two equations, whose colors correspond. The experimental data are in good agreement with Žukauskas's experiment, and Eq. (10) and Eq. (11) can predict a single-phase friction factor within a deviation of ± 4%.

3.4.2 Friction Factor with Falling Film Liquid

The pressure drop under spray conditions is influenced by the resistance from the tube bundle and friction at the interface of the air and falling film liquid. Combined with Eqs. (6)-(8), the friction factor under spray conditions can be expressed as:

$$f = f_{tb} + f_{\Gamma} \tag{13}$$

The spray friction factor, f_{Γ}, is influenced by friction at the interface between the air and falling film liquid, which indicates that the expression of the spray friction factor should be related to the Reynolds number of both the air and falling film liquid. According to the research of Liu et al. (2014), the expression of the spray friction is as follows:

$$f_{\Gamma} = B \cdot Re_g^{n_1} Re_{\Gamma}^{n_2} \tag{14}$$

where B, n_1 and n_2 are constants to be determined. According to Eq. (9), (12) and (13), the correlation form of the friction factor with falling film liquid is as follows:

$$f = A \cdot Re_g^{m} + B \cdot Re_g^{n_1} Re_{\Gamma}^{n_2} \tag{15}$$

Based on the experimental data and the correlations of single-phase friction factors, the prediction correlations of the friction factor with the falling film liquid are obtained.

For counter flow:

$$f_{ctr} = 6.287 Re_g^{-0.3057} + 0.0309 \cdot Re_g^{-0.7539} Re_{\Gamma}^{1.3448} \tag{16}$$

For cocurrent flow:

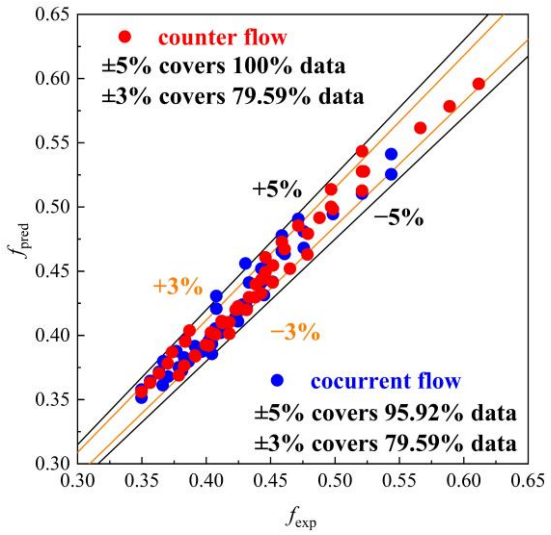

Fig. 12 Comparison between the experimental values of *f* and the predictions of Eq. (16) and Eq. (17) on the spray condition

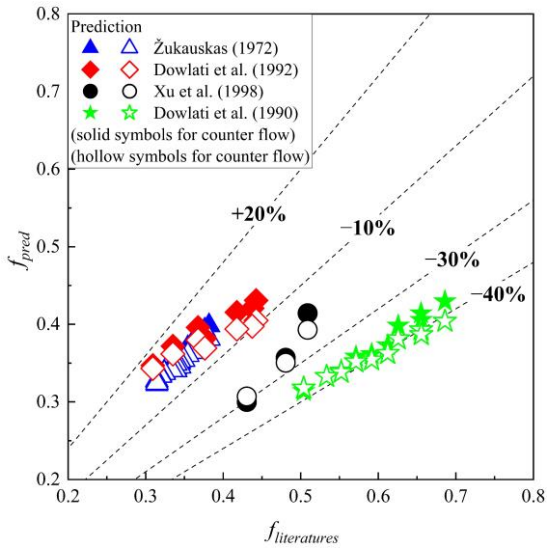

Fig. 13 Comparison between *f* in the literature and the predictions calculated by Eq. (16) and Eq. (17)

$$f_{prl} = 3.1511 Re_g^{-0.2340} + 0.0065 \cdot Re_g^{-0.6849} Re_{\Gamma}^{1.4706} \tag{17}$$

The correlations are adapted for the following conditions: staggered arrangement with an *s/D* value of 1.6, Re_g of value 6284~16233 and Re_{Γ} value of 233~462. The corresponding air velocity is 2.5~6.4 m/s, and the spray density is 0.056~0.111 kg/(m·s). The correlations for counterflow and cocurrent flow both perform well, with a deviation between the predicted and experimental *f* value of ±3%, covering 79.59% of the data for both counterflow and cocurrent flow. This proportion is 95.92% in the range of ±5% deviation for cocurrent flow, whereas all the data for counterflow can be predicted within ±5% deviation, as shown in Fig. 12.

The prediction of the single-phase pressure drop correlation is compared with experimental data from other studies, as shown in Fig. 13. The predicted *f* value

Table 5 Experimental conditions in other research

scholars	Tube diameter D [mm]	Relative tube pitch s/D	tube arrangement
Žukauskas (1972)	38	1.6	triangular staggered
Dowlati et al. (1992)	12.7	1.75	triangular staggered
Xu et al. (1998)	9.79	1.28	in-line square
Dowlati et al. (1990)	19	1.3	triangular staggered

calculated by the prediction equation of the counter flow, Eq. (10), is represented by solid points, whereas that of the cocurrent flow, Eq. (11), is represented by hollow points. The experimental conditions of these studies are summarized in Table 5. The prediction equations of the friction factor for counter flow and cocurrent flow both have great accuracy, with deviations of −10% to +20% on the data from Žukauskas (1972) and Dowlati et al. (1992), and a slightly lower prediction on the data from Xu et al. (1998) and Dowlati et al. (1990). Although the in-line square is used in Xu's experiments, which is regarded as a less-resistant tube arrangement, the tube pitch of 1.28 is much smaller than that of this study, which results in less air flowing area and more resistance from the tube bundle. Thus, the prediction f is lower than that in Xu's experiments. The tube pitch of the experimental data in Dowlati et al. (1990) is 1.3, and the tubes are in a triangular staggered arrangement, which further decreases the flow area and causes a larger friction factor than the in-line square arrangement does. Thus, the accuracy of correlations is strongly influenced when the tube pitch is too small, and adding parameters related to tube pitch to correlations is suggested in future studies.

4. CONCLUSIONS

In the present study, the pressure drop of the air flowing across the horizontal tube bundle with falling film water is investigated experimentally, and the effects of the air velocity, spray density of the falling film water and flow direction are analyzed. The prediction correlation of the friction factor under different conditions is reported, including nonspray/spray and counter/cocurrent flow conditions, which are in great agreement with the experimental data from other studies. The following conclusions are drawn:

(1) The pressure drop under spray conditions is significantly greater than that observed under nonspray conditions. This is attributed to a reduction in the flow area of the air, resulting in an increased relative velocity between the air and water, which in turn leads to an elevated pressure loss. Additionally, the liquid film induces shear and direct impacts between the air and water, leading to an increase in pressure loss.

(2) The pressure drop increases with the air velocity and spray density of the water and is slightly greater under counterflow conditions than under cocurrent flow conditions. The counter air flow has a greater relative velocity with the falling film, and it has greater effects on the direct contact between the air and the falling film. The spray pressure drop ΔP_Γ accounts for approximately 10~30% and 10~25% of the total pressure drop of the counter flow and cocurrent flow, respectively. The reason for the slight differences in the effects of counter flow and cocurrent flow on the pressure drop is that the relative velocities of the air and spray water may be similar for these two flows. In addition, a low/high-disturbance region is proposed to explain the variation in the spray pressure drop with the air velocity and spray density.

(3) The prediction correlations of the air single-phase friction factor and friction factor on the spray condition are obtained for counter flow and cocurrent flow. The correlations for the single-phase friction factor can predict experimental data within a deviation of ±4% and are in good agreement with Žukauskas's research. The correlations for the friction factor under spray conditions can predict almost all the data within ±5% deviation.

ACKNOWLEDGEMENTS

The research is supported by the National Natural Science Foundation of China (No. 51936002).

CONFLICT OF INTEREST

The authors declare no conflict of interest.

AUTHORS CONTRIBUTION

Chao Li: Data curation, Formal analysis, Investigation, Methodology, Writing-original draft, Writing-review & editing. **Xiankai Zhang**: Data curation, Methodology, Investigation. **Yali Guo**: Methodology, Writing review & editing. **Shengqiang Shen**: Funding acquisition, Supervision, Writing-review & editing. **Qinggang Qiu**: Writing-review & editing.

REFERENCES

Anderson, N. R. (2014). *Evaluation of the performance characteristics of a hybrid (dry/wet) induced draft dephlegmator* [Doctoral dissertation, Stellenbosch University]. https://scholar.sun.ac.za/items/04e87b55-00dc-4abf-8d51-7d2910c2627e

Catrawedarma, I., & Deendarlianto, I. (2020). The performance of airlift pump for the solid particles lifting during the transportation of gas-liquid-solid three-phase flow: a comprehensive research review. *Journal of Process Mechanical Engineering*, *235*(2), 606-628. https://doi.org/10.1177/0954408920951728

Catrawedarma, I., & Deendarlianto, I. (2022). Hydrodynamic behaviors of air-water two-phase flow during the water lifting in a bubble generator

type of airlift pump system. *Heat and Mass Transfer*, *58*(6), 1005-1026. https://doi.org/10.1007/s00231-021-03157-z

Dowlati, R., Chan, A. M. C., & Kawaji, M. (1992). Hydrodynamics of two-phase flow across horizontal in-line and staggered rod bundles. *Journal of Fluids Engineering*, *114*(3), 450-456. https://doi.org/10.1115/1.2910052

Dowlati, R., Kawaji, M., Chan, A. M. C. (1990). Pitch-to-diameter effect on two-phase flow across an in-line tube bundle. *Aiche Journal*, *36*(5), 765-772. https://doi.org/10.1002/aic.690360513

Finlay, I. C., Harris, D. (1984). Evaporative cooling of tube banks. *International Journal of Refrigeration*, *7*(4), 214-224. https://doi.org/10.1016/0140-7007(84)90073-2

Fiorentino, M., Starace, G. (2016). Numerical investigations on two-phase flow modes in evaporative condensers. *Applied Thermal Engineering*, *94*, 777-785. https://doi.org/10.1016/j.applthermaleng.2015.10.099

Heyns, J. A., Kröger, D. G. (2010). Experimental investigation into the thermal-flow performance characteristics of an evaporative cooler. *Applied Thermal Engineering*, *30*(5), 492-498. https://doi.org/10.1016/j.applthermaleng.2009.10.010

Kline, S. J. (1985). The purposes of uncertainty analysis. *Journal of Fluids Engineering*, *107*(2), 153-160. https://doi.org/10.1115/1.3242449

Liu, H., Shen, S. Q., Gong, L. Y., Chen, S. (2014). Shell-side two-phase pressure drop and evaporation temperature drop on falling film evaporation in a rotated square bundle. *Applied Thermal Engineering*, *69*(1-2), 214-220. https://doi.org/10.1016/j.applthermaleng.2013.11.061

Mizushina, T., Ito, R., Miyashita H. (1967) Experimental Study of Evaporative Cooler. *Kagaku Kogaku Ronbunshu*, *31*, 469-473. https://doi.org/10.1252/KAKORONBUNSHU1953.31.469

Plessis, J. D., Owen, M. (2020). An Experimental Investigation of the Air-Side Pressure Drop Through a Bare Tube Bundle. *Journal of Thermal Science and Engineering Applications*, *12*(1), 011012. https://doi.org/10.1115/1.4044425

She, Y., Chan, W., Chang, F., Guo, K., Li, H. (2021). Experimental investigation on the characteristics of pressure drop and air/vapor flow over horizontal tube bundle with water-spray falling film. *Desalination and Water Treatment*, *216*, 34-46. https://doi.org/10.5004/dwt.2021.26818

Skundric, J., Zivkovic, P., Tica, M., Tomic, M., Barz, C. (2023). Investigation of air-cooled condenser's operating parameters in modern thermal power plant. *Thermal Science*, *27*(3B), 2477-2487. https://doi.org/10.2298/TSCI220806203S

Xu, G. P., Tso, C. P., Tou, K. W. (1998). Hydrodynamics of two-phase flow in vertical up and down-flow across a horizontal tube bundle. *International Journal of Multiphase Flow*, *24*(8), 1317-1342. https://doi.org/10.1016/S0301-9322(98)00035-4

Zalewski, W., Gryglaszewski, P. A. (1997). Mathematical model of heat and mass transfer processes in evaporative fluid coolers. *Chemical Engineering and Processing*, *36*(4), 271-280. https://doi.org/10.1016/S0255-2701(97)00006-8

Zhang, P., Guo, B., Wang, L. (2023). An Experimental Study on the Heat and Mass Transfer Characteristics of an Evaporative Cooler. *Energies*, *16*(21), 7330. https://doi.org/10.3390/en16217330

Žukauskas, A. (1972). Heat Transfer from Tubes in Crossflow. *Advances in Heat Transfer*, *8*, 93-160. https://doi.org/10.1016/S0065-2717(08)70038-8